Development of inhomogeneous conduction electron spin polarization in the antiferroquadrupolar phase of UPd_3

2002 J. Phys.: Condens. Matter 14 4595

(http://iopscience.iop.org/0953-8984/14/17/329)

INSTITUTE OF PHYSICS PUBLISHING JOURNAL OF PHYSICS: CONDENSED MATTER

J. Phys.: Condens. Matter **14** (2002) 4595–4609 PII: S0953-8984(02)32397-X

Development of inhomogeneous conduction electron spin polarization in the antiferroquadrupolar phase of UPd_3

A Schenck[1], **F N Gygax**[1] **and K A McEwen**[2]

[1] Institute for Particle Physics of ETH Zürich, CH-5232 Villigen PSI, Switzerland
[2] Department of Physics and Astronomy, University College London, London WC1 E6BT, UK

Received 7 January 2002
Published 18 April 2002
Online at stacks.iop.org/JPhysCM/14/4595

Abstract

We have measured the Knight shift and inhomogeneous line broadening of positive muons implanted in monocrystalline UPd_3 from 2 K up to 300 K. We find two components in the transverse-field ($H_{ext} = 0.6$ T) precession signal with amplitude ratio 2:1, which is independent of temperature up to 300 K. The two signals are associated with two different muon sites with axial symmetry. Both the Knight shifts and the relaxation rates show pronounced anomalies at the critical temperatures of $T_2 \simeq 4.4$ K, believed to reflect, *inter alia*, a magnetic transition, $T_1 \simeq 6.8$ K and $T_0 \simeq 7.6$ K, originating from antiferroquadrupolar ordering. Details depend on sample orientation and signal component. It is argued that the particular temperature dependence of both the Knight shift and the inhomogeneous line broadening of the stronger component below 10 K is associated with the contact hyperfine contribution to the Knight shift and reflects an inhomogeneous conduction electron spin polarization caused by the antiferroquadrupolar order. Additional zero-field μSR measurements yield a very small temperature-independent relaxation rate consistent with the field inhomogeneity arising from the Pd nuclear dipole fields. In particular, below 4.5 K there is no evidence for additional static fields due to a magnetically ordered state.

1. Introduction

As time progresses more and more rare-earth and U-based intermetallic compounds have been discovered to show a non-magnetic type of ordering which is associated with the quadrupole moment of a non-spherical 4f- or 5f-electron charge distribution around their respective atoms [1]. With a few exceptions the same compounds also show magnetic order, usually developing below the onset temperature of the quadrupolar order. The quadrupolar order leads to tiny periodic lattice distortions which may be detected by superlattice peaks in elastic neutron scattering, although of course, the neutrons do not couple directly to the quadrupolar

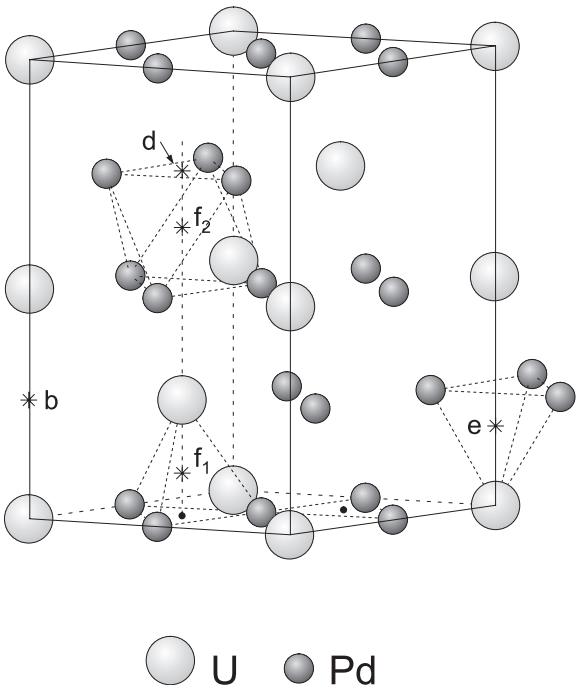

Figure 1. Crystal structure of dhcp UPd_3. The quasi-cubic U sublattice is built up from the a sites (generic positions (000), $(00\frac{1}{2})$) and the hexagonal U sublattice from the c sites (generic positions $(\frac{1}{3}\,\frac{2}{3}\,\frac{1}{4})$, $(\frac{2}{3}\,\frac{1}{3}\,\frac{3}{4})$). Indicated are the possible interstitial sites of the μ^+: b, d, f_1, f_2 and e (Wyckoff notation).

moments. The same restriction applies to the spin-$\frac{1}{2}$ muon probe which interacts through its magnetic moment only magnetically with its environment and is blind to the details of the charge distribution on some neighbouring host atoms. Nevertheless, one may ask whether there are also some indirect mechanisms which allow us to monitor quadrupolar phase transitions by μSR spectroscopy. So far the only compound where a transition into the quadrupolar-ordered state could be clearly seen by means of muons is CeB_6 [2,3]. However, in this case an external field had to be present which is known to induce some sort of antiferromagnetic (AFM) order below the quadrupolar ordering temperature T_Q [4]. Hence what is probably seen in the μSR measurements is primarily the onset of the induced AFM order although the results appear as yet to be inconsistent with NQR and neutron scattering data. In this work we present and discuss μSR measurements on the compound UPd_3 which clearly shows significant anomalies at the low-temperature transitions associated with quadrupolar order. Preliminary results were published in [5].

UPd_3 is a particularly interesting system since it is an intermetallic compound in which the uranium 5f electrons have a well-localized character. This localized nature is manifested by the clear observation, using inelastic neutron spectroscopy, of dispersive crystal-field-type excitations (magnetic excitons) at low temperatures [6, 7]. The crystal structure of UPd_3 is double-hexagonal close packed, with U ions at sites having locally hexagonal and locally quasi-cubic symmetry (see figure 1). Bulk property measurements of the heat capacity [8], magnetic susceptibility and thermal expansion of UPd_3 [9–11] showed evidence of two phase transitions around 7 and 5 K. Subsequent studies of the heat capacity and thermal expansion [12] showed

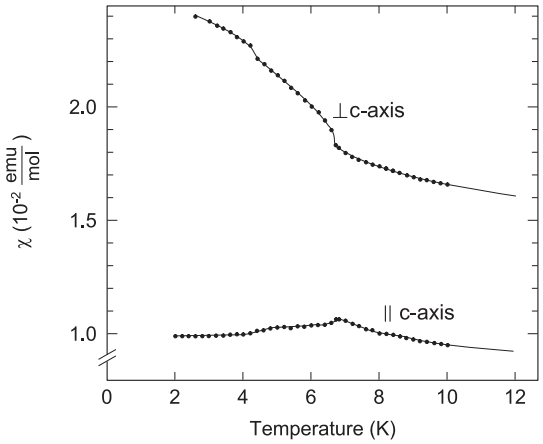

Figure 2. Low-temperature behaviour of the bulk magnetic susceptibility for $H_{ext} \parallel b$-axis and $H_{ext} \parallel c$-axis.

evidence of three phase transitions at $T_0 = 7.6$ K, $T_1 = 6.8$ K and $T_2 = 4.4$ K. Elastic constant and ultrasonic attenuation work [13] revealed that the T_1-transition is actually split into two transitions (denoted by T_1^+ and T_1^-) separated by about 0.2 K. However, this subtlety is not relevant to the experiments reported in the present paper.

Polarized neutron diffraction studies of UPd_3 [14] demonstrate the development of a periodic lattice distortion below T_0, with a doubling of the crystallographic unit cell. This lattice distortion is driven by the onset of ordering of the quadrupole moments of the 5f-electronic charge distributions on the U ions. The order parameter of the antiferroquadrupolar (AFQ) structures below T_0 and T_1 may be deduced from the resulting field-induced magnetic structures [15]. Definitive evidence of the AFQ order in UPd_3 was subsequently provided by the observation of resonant x-ray scattering from the aspherical charge distributions of the U ions [16]. Below T_0, the ordered quadrupole moments are predominantly on the quasi-cubic sites: the unit cell is orthorhombic with an antiphase stacking of the moments along the c-direction. Below T_1, a rotation and tilt of the quadrupoles is required to explain the x-ray and neutron results.

The transition at T_2 is accompanied by the appearance of very weak AFM ordering, together with changes in the AFQ order parameter [14, 15]. The AFM moments have a magnitude of $\sim 10^{-2}$ μ_B/U atom or less: moreover, the neutron diffraction peaks are not resolution limited, indicating that true long-range order is not present.

The quasi-cubic and hexagonal U sublattices have different magnetic susceptibilities $\overleftrightarrow{\chi}_{cub}$ and $\overleftrightarrow{\chi}_{hex}$. Polarized neutron diffraction measurements show that $\chi_{cub}^{\perp c} \simeq (3\text{–}5)\chi_{hex}^{\perp c}$ and $\chi_{cub}^{\parallel c} \gg \chi_{hex}^{\parallel c} \approx 0$ below 10 K [15, 17]. Therefore, below 10 K the quasi-cubic sublattice provides the dominant contribution to the bulk susceptibility $\overleftrightarrow{\chi}_b$, which is shown in figure 2.

2. Experimental details

The transverse-field (TF) measurements in $H_{ext} = 0.6$ T were performed with the general-purpose spectrometer GPS on the πM3 beamline of the Paul Scherrer Institute (PSI) proton accelerator facility. Some of the data were taken with the 'muons on request (MORE)' option [18] which allows the time window to be increased to 18 μs and essentially suppresses all

accidental start–stop events. The single-crystal sample, grown by the Czochralski technique, has a cylindrical shape with a diameter of 3.55 mm and a length of 4.75 mm with the crystallographic c-axis parallel to the cylinder axis. The sample was mounted in a He-flow cryostat such that it could be rotated around the c-axis with the applied field in the (a, b) plane, or around the a-axis with the field confined to the (b, c) plane. The sample was attached to the target holder by a several-centimetres-long tube made of Mylar which ensured—together with a special veto counter arrangement—that only a very small fraction of the μ^+ which failed to stop in the sample contributed to the μSR signal ($\sim$5% of all registered μ^+). Actually this small background signal was used to monitor the applied field. The applied field was precisely measured by a NMR probe placed at the position of the sample or by measuring the μ^+-precession frequency in a silver target in lieu of the UPd_3 sample. The applied field was oriented parallel to the incoming μ^+. The μ^+-polarization was turned by about 47° from horizontal to vertical by means of a spin rotator in the πM3 beamline. The TF-precession signal was measured in up, down and right directions with respect to the beamline by appropriately placed detectors. We also recorded the signal in the forward and backward directions (parallel to the applied field) to check for possible dynamically induced relaxation. No such relaxation was seen within our time window. The ZF-μSR measurements were performed with the same set-up by making use of the MORE option. In this case the initial μ^+-polarization was parallel to the μ^+-momentum and the signal was recorded in the forward and backward detectors.

3. Results

The TF-μSR signal revealed the presence of three components, as can be seen in figure 3, which displays the Fourier transform of the μSR signal taken at 6 K. The small component in the centre is the background signal discussed above and the two other strong components arise from the sample. The time evolution of the μ^+-polarization components in the up, down and right directions was generally very well fitted by the expression

$$P(t) = A(\exp(-\tfrac{1}{2}\sigma_1^2 t^2)\cos(\omega_1 t + \varphi) + \tfrac{1}{2}\exp(-\tfrac{1}{2}\sigma_2^2 t^2)\cos(\omega_2 t + \varphi)) + A_{BG}\exp(-\lambda t)\cos(\omega_{BG} t + \varphi), \quad (1)$$

where the third component accounts for the background signal. The expression implies that the amplitude ratio of the two signals from the sample is 2:1, which proved to be independent of temperature over the whole range covered (2–300 K). Henceforth the larger component is labelled as signal 1 and the smaller as signal 2.

Figure 4 displays the orientation dependence of the precession frequencies $\nu_1 = \omega_1/2\pi$ and $\nu_2 = \omega_2/2\pi$ at 6 K with the applied field $\vec{H}_{ext}$ either rotating in the (b, c) plane (a) or in the (a, b) plane (b), respectively. No further splitting is seen. The isotropy in the basal plane has important implications concerning the possible μ^+-sites, as will be discussed further on.

From the frequencies ν_1 and ν_2, the Knight shifts K_1 and K_2 were extracted in the usual way by correcting for the demagnetization and Lorentz fields. The demagnetization factors $N_{\parallel,\perp}$ for $\vec{H}_{ext} \parallel c$-axis and $\vec{H}_{ext} \perp c$-axis were estimated from the tables in [19] ($N_\parallel/4\pi \simeq 0.22$, $N_\perp/4\pi \simeq 0.41$). The bulk susceptibility was taken from [10]. Figure 5 displays the Knight shifts, obtained in this way, for the two signals for $\vec{H}_{ext} \parallel c$-axis and $\vec{H}_{ext} \perp c$-axis. As an example, figure 6 displays the fitted relaxation rate σ_1 for $\vec{H}_{ext} \perp c$-axis. We particularly note the pronounced increase of σ_1 below $\sim$10 K. This is seen for all σ_i, except for $\sigma_1^\parallel$ for $\vec{H}_{ext} \parallel c$-axis (see also figures 8(b), 9(b) and 10). The relaxation rates become much smaller in lower fields, e.g. in a transverse field of 100 G the fitted σ is of the order of 0.06 μs^{-1} (no splitting in such a small field) and is of the same magnitude as in zero field (ZF) (see below). The observed transverse-field relaxation rate at 0.6 T is thus clearly

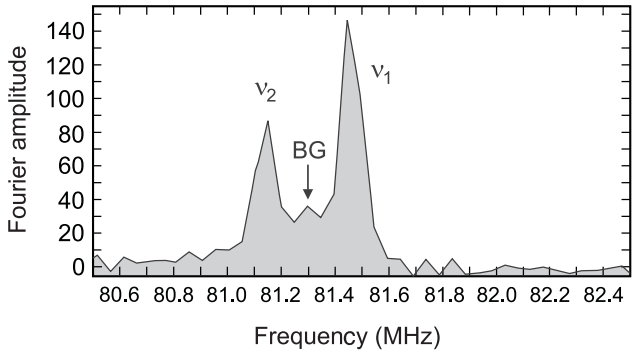

Figure 3. The Fourier transform of the TF-μSR spectrum taken at 6 K and $H_{ext} = 0.6$ T. The small peak, labelled BG, between the two signals from the sample, is the background signal.

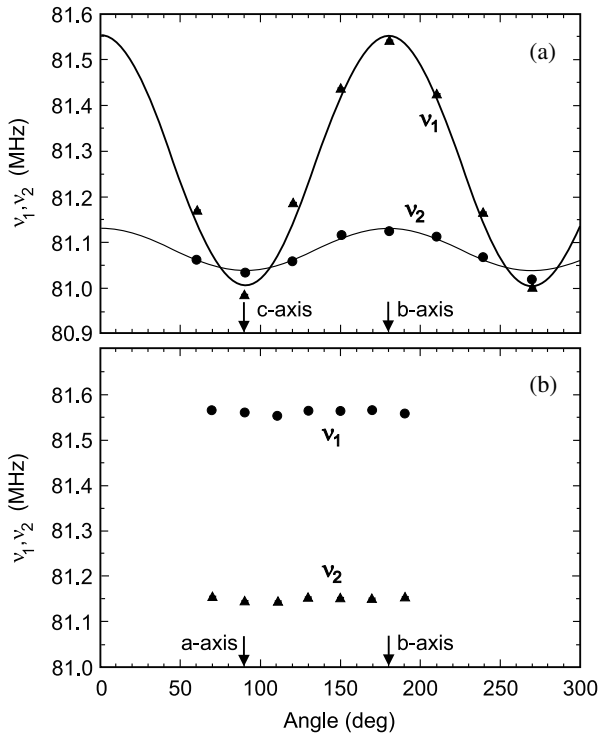

Figure 4. Orientation dependence of the two frequencies ν_1 and ν_2 for H_{ext} rotating (a) in the (c, b) plane, (b) in the (a, b) plane. The solid curves represent $\cos^2(\theta)$ fits.

field induced (inhomogeneous line broadening) and reflects a certain enhanced width of the internal fields at the two muon sites.

Finally figure 7 displays the temperature dependence of the relaxation rate σ of the ZF signal which was best fitted by a Gaussian or Gaussian Kubo–Toyabe function. As can be seen, there is no change in σ from 1.8 K up to 20 K. The relaxation is fully quenched in a longitudinally applied field of 100 G confirming the static origin of the ZF relaxation.

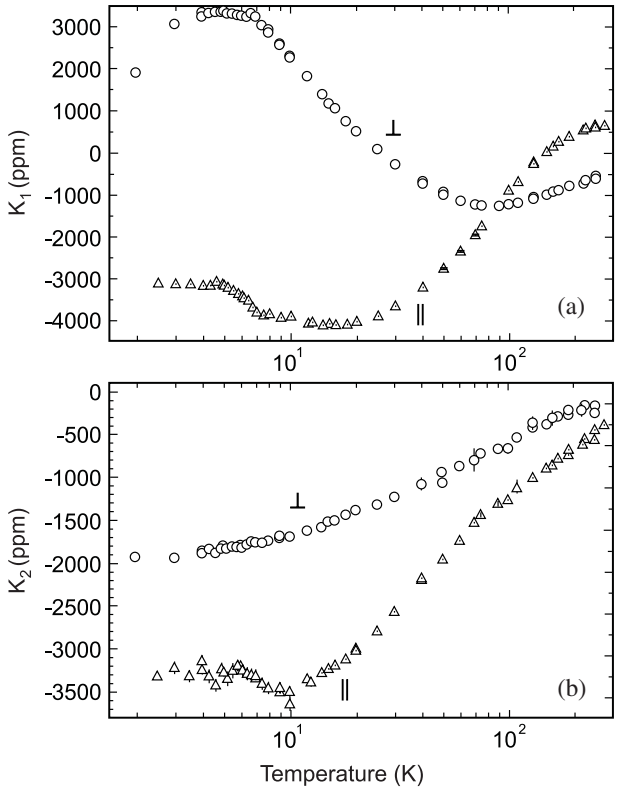

Figure 5. Temperature dependence of the Knight shifts K_1 and K_2, deduced from the frequencies ν_1 and ν_2, for different crystal orientations: $\|$ denotes $\vec{H}_{ext}$ parallel to the c-axis; $\perp$ denotes $\vec{H}_{ext}$ perpendicular to the c-axis.

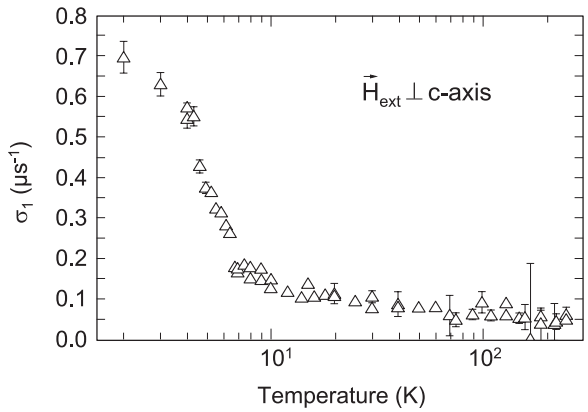

Figure 6. Temperature dependence of the relaxation rate σ_1 for $\vec{H}_{ext} \perp c$-axis.

4. Discussion of the general temperature dependence of the Knight shifts and muon sites

We begin with a consideration of the angular dependencies of K_1 and K_2 (see figure 4). The shifts K_i arise basically from two contributions:

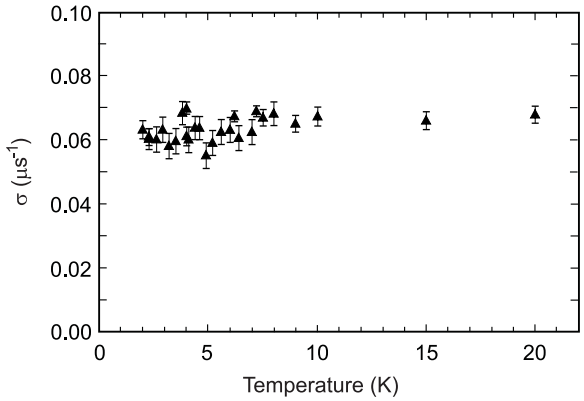

Figure 7. Temperature dependence of the ZF-relaxation rate σ. The initial μ^+-polarization is directed perpendicular to the c-axis.

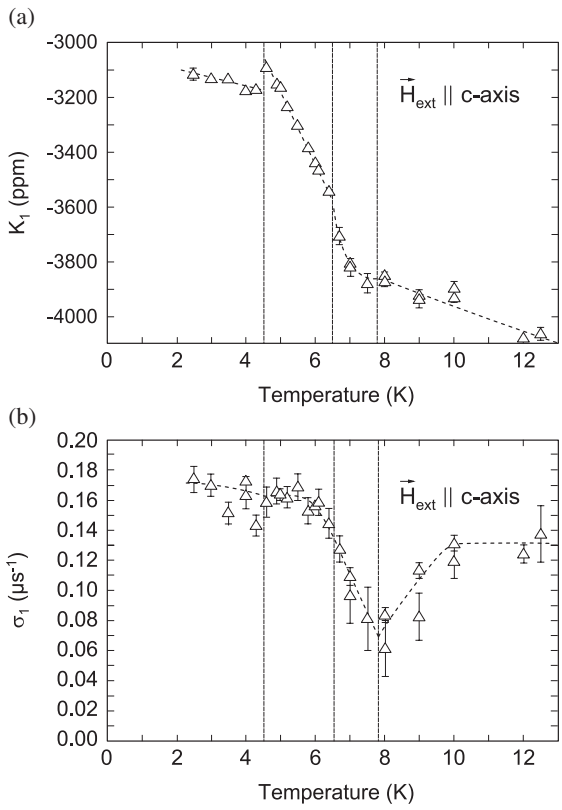

Figure 8. Low-temperature behaviour of (*a*) $K_1^{\parallel}$ and (*b*) $\sigma_1^{\parallel}$. The vertical dashed lines mark the positions of T_0, T_1 and T_2. To guide the eye the data points are smoothly interpolated by the dashed lines.

(i) the dipolar field originating from the local moments induced by the applied field; and
(ii) the contact hyperfine field at the μ^+ due to the spin polarization of the conduction electrons arising via the RKKY mechanism from the induced local moments on the f-electron atoms.

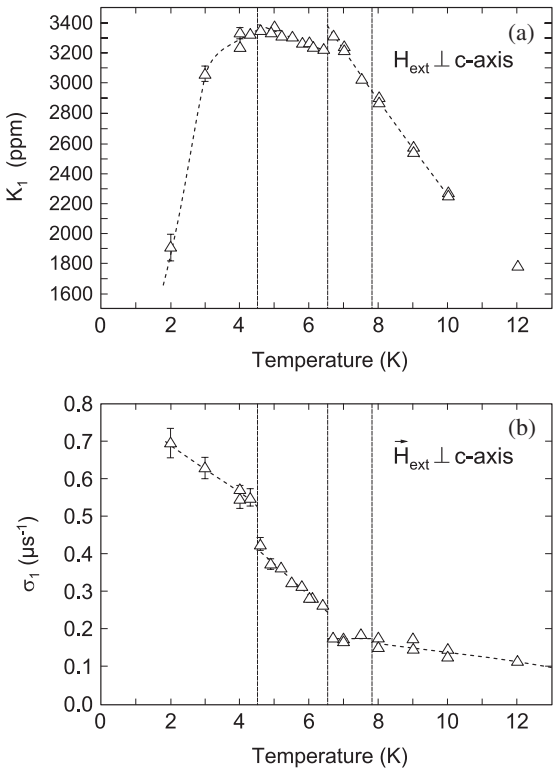

Figure 9. Low-temperature behaviour of (*a*) $K_1^{\perp}$ and (*b*) $\sigma_1^{\perp}$. See also the caption of figure 8.

Thus we write [20]

$$K = K_{dip} + K_c + K_0, \tag{2}$$

with

$$K_{dip} = \vec{h} \cdot \overleftrightarrow{A}_{dip} \cdot \overleftrightarrow{\chi}_f \cdot \vec{h}, \tag{3}$$

$$K_c = A_c \vec{h} \cdot \overleftrightarrow{\chi}_f \cdot \vec{h}. \tag{4}$$

Here $\vec{h}$ is a unit vector along $\vec{H}_{ext}$, $\overleftrightarrow{\chi}$ is the susceptibility tensor associated with the f electrons, $\overleftrightarrow{A}_{dip}$ is the dipolar coupling tensor and A_c the contact coupling constant, conventionally believed to be a scalar and temperature independent. All the temperature dependence of K rests with $\overleftrightarrow{\chi}_f$. K_0 in equation (2) accounts for a possible temperature-independent contribution to the Knight shift. The expressions (3) and (4) imply that the f-electron atoms are crystallographically equivalent and that the bulk susceptibility is given by a unique $\overleftrightarrow{\chi}$. This is not true in the present case since there are two distinct U sublattices, as mentioned in the introduction, and each sublattice responds differently to the applied field and, of course, couples differently to the muon. Therefore equations (3) and (4) should be replaced by

$$K_{dip} = \vec{h} \cdot (\overleftrightarrow{A}_{dip,hex} \cdot \overleftrightarrow{\chi}_{hex} + \overleftrightarrow{A}_{dip,cub} \cdot \overleftrightarrow{\chi}_{cub}) \cdot \vec{h}, \tag{5}$$

$$K_c = A_{c,hex}(\vec{h} \cdot \overleftrightarrow{\chi}_{hex} \cdot \vec{h}) + A_{c,cub}(\vec{h} \cdot \overleftrightarrow{\chi}_{cub} \cdot \vec{h}), \tag{6}$$

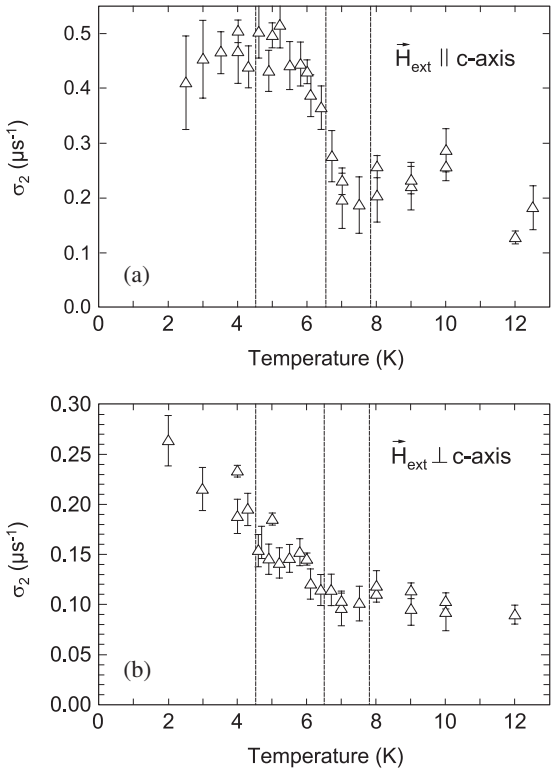

Figure 10. Low-temperature behaviour of (*a*) $\sigma_2^{\parallel}$ and (*b*) $\sigma_2^{\perp}$. In comparison to figures 8 and 9 anomalies at T_0, T_1 and T_2 are much less pronounced or absent.

where $\overleftrightarrow{\chi}_{hex}$ and $\overleftrightarrow{\chi}_{cub}$ refer to the hexagonal and cubic U sublattices, respectively, and $\overleftrightarrow{\chi}_{bulk}=\overleftrightarrow{\chi}_{hex}+\overleftrightarrow{\chi}_{cub}$, neglecting other smaller contributions. The isotropy of K_1 and K_2 in the basal plane implies now that $\overleftrightarrow{A}_{dip}$ is of the form

$$\overleftrightarrow{A}_{dip}=\begin{pmatrix} -\frac{1}{2} & 0 & 0 \\ 0 & -\frac{1}{2} & 0 \\ 0 & 0 & 1 \end{pmatrix} A_{dip}. \tag{7}$$

This in turn implies that the μ^+ are located at axially symmetric sites. Interstitial sites with this property are the b, d, e and f sites with the generic positions $(0, 0, \frac{1}{4})$, $(\frac{1}{3}, \frac{2}{3}, \frac{3}{4})$, $(0, 0, z)$ and $(\frac{1}{3}, \frac{2}{3}, z)$ [21, 22].

Inspecting figure 1, one notices that there are actually two distinct f sites: the f_1 site with $z \simeq 0.066$ (centre of the tetrahedron made up of one hexagonal U atom and three Pd atoms) and the f_2 site with $z = 5/8$ (centre of the octahedron made up of six Pd atoms). Note that the e site resembles very much the f_1 site except that the nearest U neighbour is of the quasi-cubic type (see figure 1). Calculated A_{dip} for these sites are collected in table 1. Concerning the tetrahedral sites e and f_1, it is assumed that the μ^+ would take up a position such that the distance to the four nearest neighbours is equal ($\sim$1.8 Å). The multiplicity of the sites is four for the e and f sites and two for the b and d sites. Given the ratio of two for the amplitudes of the signals 1 and 2, we may conclude that the first component is associated with the f and/or e sites and the second component with the b and/or d sites. According to [22] the octahedral

Table 1. Compilation of dipolar coupling constants A_{dip} (kG/μ_B) for various interstitial sites in Wyckoff notation.

Site/multiplicity	Position	A_{dip}^{cub}	A_{dip}^{hex}
b/2	$(00\frac{1}{4})$	2.522	−0.594
d/2	$(\frac{1}{3}\frac{2}{3}\frac{3}{4})$	0.007	−0.483
e/4	000.18	4.05	−0.485
f_1/4	$(\frac{1}{3}\frac{2}{3}0.058)$	−0.510	2.935
f_2/4	$(\frac{1}{3}\frac{2}{3}5/8)$	−0.270	−0.008

f_2 site possesses the largest interstitial volume. But it is not an entirely symmetric site since the nearest-neighbour hexagonal U-atom arrangement along the *c*-axis direction is not symmetric (see figure 1). The nearest fully symmetric site would be the d site. On the other hand, the very spacious b site may not provide a deep enough potential well in contrast to the tetrahedral e site. In fact the b site is not even mentioned in [22] as a possible site for hydrogen in UPd_3. Hence we may conclude that the stronger signal 1 arises from μ^+ located at the f_1 or the e site, while the weaker signal 2 arises most probably from μ^+ located at the d site (which is also not considered in [22]). Inspecting table 1 it is seen that for the d site the cubic U sublattice A_{dip}^{cub} is nearly zero. This suggests that the Knight shift K_2 arises predominantly from the hexagonal U sublattice (see figure 5). Not inconsistent with a predominantly hexagonal U-sublattice origin of $K_2(T)$ is the absence of any pronounced anomalies at T_0, T_1 and T_2, in contrast to the behaviour of $K_1(T)$. However, the temperature dependence of K_2 for both orientations (see figure 5) is quite different from that of $\overleftrightarrow{\chi}_{hex}(T)$ and points to muon-induced changes of the CEF splitting of the nearest U neighbours [23]. The same is then expected also for the nearest U neighbours in the quasi-cubic sublattice. This circumstance renders it impossible to extract from $K_1(T)$ and $K_2(T)$ the dipolar coupling parameters and hence to determine unambiguously the actual μ^+-sites.

5. Discussion of the anomalies of K_1 and σ_1 at low temperatures

In the following we discuss qualitatively the results obtained below ∼10 K. The discussion will be restricted to the behaviour of $K_1(T)$ and $\sigma_1(T)$ since the low-temperature anomalies are most pronounced in the dominant signal 1. Concerning $K_2(T)$ see the remarks in section 4. Figures 8, 9 show $K_1(T)$ and $\sigma_1(T)$ on an extended scale for $\vec{H}_{ext} \parallel c$-axis and $\vec{H}_{ext} \perp c$-axis. For $\vec{H}_{ext} \parallel c$-axis, both $K_1(T)$ and $\sigma_1(T)$ reveal anomalies at T_0, T_1 and T_2 (see figure 8). For $\vec{H}_{ext} \perp c$-axis, anomalies are only visible at T_1 and T_2. The anomalies consist of step-like changes, or of changes in the slopes of the temperature dependence. Particularly striking are the step-like changes in $\sigma_1^{\perp}(T)$ for $\vec{H}_{ext} \perp c$-axis of ∼39% at T_1 and ∼21% at T_2. Note also the overall drastic increase of $\sigma_1(T)$ below 10 K (figure 6): $\sigma_1^{\perp}(2\text{ K})/\sigma_1^{\perp}(10) \simeq 4.7$ whilst $\chi_{cub}^{\perp}(2\text{ K})/\chi_{cub}^{\perp}(10\text{ K}) \simeq 1.8$ [15] (see also figure 2). We also notice that $|K_1^{\parallel}(T)|$ increases effectively linearly with temperature between T_1 and T_2, while $K_1^{\perp}$ in the same regime is nearly temperature independent. This is in contrast to $\sigma_1^{\parallel}$ and $\sigma_1^{\perp}$ which show an opposite behaviour, more parallel to $\chi_b^{\parallel}(T)$ and $\chi_b^{\perp}(T)$, although $\sigma_1^{\parallel,\perp}(T)$ does not scale with $\chi_b^{\parallel,\perp}(T)$ or $\chi_{cub}^{\parallel,\perp}(T)$, respectively. The dramatic decrease of $K_1^{\perp}(T)$ below T_2 in contrast to the near temperature independence of $K_1^{\parallel}(T)$ in the same regime is striking.

The measured $\overleftrightarrow{\chi}_{cub}$ (and $\overleftrightarrow{\chi}_{hex}$) are not precise enough to determine their relative changes at T_0, T_1 and T_2 reliably. However, since $\overleftrightarrow{\chi}_{cub}$ dominates the bulk susceptibility below 10 K, we

may assume that the relative changes of $\overleftrightarrow{\chi}_b$ at T_1 and T_2 reflect well $\overleftrightarrow{\chi}_{cub}$ (no anomalies in $\overleftrightarrow{\chi}_b$ are seen at T_0). Figure 2 shows that at T_2, $\Delta\chi^{\parallel} \simeq 0, \Delta\chi^{\perp} \simeq 1.8\%$ and at T_1, $\Delta\chi^{\parallel} \simeq 0, \Delta\chi^{\perp} \simeq 2.7\%$. Comparing these changes with the relative changes of $K_1(T)$ and $\sigma_1(T)$, it appears that it is not primarily the susceptibility which governs the behaviour of $K_1(T)$ and $\sigma_1(T)$ (at T_2, $\Delta K_1^{\parallel} \simeq -3.8\%$, $K_1^{\perp}$ changes only in slope, $\Delta\sigma_1^{\parallel} \simeq 0$, $\Delta\sigma_1^{\perp} \simeq +21\%$; at T_1, $K_1^{\parallel}$ changes only in slope, $\Delta K_1^{\perp} \simeq -5\%$, $\Delta\sigma_1^{\parallel} \simeq 0, \sigma_1^{\perp} \simeq +39\%$; at T_0, $K_1^{\parallel}$ changes only in slope, $K_1^{\perp}$ shows no anomaly; $\sigma_1^{\parallel}$ shows a drastic change in slope and $\sigma_1^{\perp}$ shows a slight change in slope; the sign $+/-$ indicates increase/decrease when crossing the critical temperature from above).

What, then, is the origin of the inhomogeneous line broadening in the quadrupolar ordering regime? Note that above 15 K all σ_i show values below 0.1 μs^{-1}, i.e. approach the value of 0.06 μs^{-1} also found in the ZF data (see figure 7). Hence above 15 K there is little additional induced line broadening beyond that induced by the Pd nuclear dipole fields. This demonstrates the high quality of our sample and indicates that the much increased $\sigma_1^{\perp}$ (also $\sigma_2^{\parallel}$ and $\sigma_2^{\perp}$; see figure 10) below 10 K is of intrinsic origin. In other words the increased inhomogeneous line broadening reflects the development of non-uniformly distributed fields at the μ^+-sites, apparently driven by the onset of quadrupolar order. Since the quadrupolar order is accompanied by a modulated lattice distortion it is reasonable to expect that this distortion might lead to a distribution of dipole fields and possibly also contact hyperfine fields at the μ^+-sites. However, on closer inspection the distortions are much too small (c/a changes by only -6×10^{-5} [9]) to be responsible for the observed line broadening below 10 K. Another source of line broadening is the possibility, as suggested by neutron scattering studies in a field of 4 T, that there is a field-induced AFM order in addition to the uniform ferromagnetic response already below T_0, involving primarily the quasi-cubic U sites [15]. For $T < T_1$ it is suggested that if $\vec{H}_{ext}$ is applied parallel to the a-axis, moments perpendicular to $\vec{H}_{ext}$ along the c-axis are induced. To avoid frustration the induced moments must be ferromagnetically ordered in the basal plane and alternate in direction along the c-axis. Therefore, along the c-axis, the net induced moment will be symmetrically and periodically tilted away from $\vec{H}_{ext}$ by a certain angle. However, it is easy to see that both at the f_1 site and the e site this type of staggered moment arrangement produces unique dipole and contact fields and no splitting or broadening of the μSR signal will occur.

In any case the broadening must involve the induced dipolar fields and/or the contact hyperfine fields. A hint that the dipolar fields cannot be involved derives from the huge change of $\sigma_1^{\perp}(T)$ across T_1: since the relevant A_{dip}^{cub} is a fixed constant and $\chi_{cub}^{\perp}$ changes probably only by few per cent across T_1, the change in $\sigma_1^{\perp}(T)$ must have another origin.

The remaining possibility is that the inhomogeneous line broadening is associated with the contact hyperfine field, which implies that the conduction electron spin polarization is not uniformly distributed. This is not altogether impossible since the conduction electron spin polarization is induced via the RKKY interaction by the local f-electron moment. If the overlap of the s-wave-type conduction electrons, screening the μ^+-charge, with the non-spherical 5f-electron distribution depends on the orientation of the 5f-electron density distribution it is natural to expect the spin polarization at the μ^+ to become a function of the orientation of the 5f wavefunction, i.e. of the orientation of the quadrupole moment [24]. In the quadrupolar phase below T_1 (or T_0) the quadrupole moments may assume up to four different orientations [15,16] and hence one may expect to find different contact coupling constants. In principle, this should lead to a further splitting of the μSR signal, which may not be resolvable, and all that might be observed is a line-broadening effect. To explore fully all possibilities we write K_c in the following form by permitting that each CEF level couples differently to the conduction electrons [25]:

$$K_c = \sum_{i=1}^{9} A_{c,i}\chi_{CEF,i}, \tag{8}$$

where $\chi_{CEF,i}$, the susceptibility associated with the ith CEF level, is given by the Van Vleck expression

$$\chi^{\alpha}_{CEF,i} = \frac{N_a(\mu_B g_J)^2}{Z}\left[|\langle i|J_\alpha|i\rangle|^2\frac{\exp(-E_i/kT)}{kT} + \sum_{j\neq i}|\langle i|J_\alpha|j\rangle|^2\frac{(1-\exp(-\Delta_{ij}/kT))}{\Delta_{ij}}\mathrm{e}^{-E_i/kT}\right], \tag{9}$$

with $\Delta_{ij} = E_j - E_i$, $Z = \sum_{i=1}^{9}\exp(-E_i/kT)$. α denotes a particular Cartesian direction (x, y, z). The exchange interaction between neighbouring U atoms may further modify the susceptibility terms, which may be taken into account by writing

$$\chi^{\alpha}_{i} = \frac{\chi^{\alpha}_{CEF,i}}{1-\lambda^{\alpha}_{i}\chi^{\alpha}_{CEF,i}}, \tag{10}$$

where λ^{α}_{i} is a molecular-field parameter. According to the RKKY mechanism the coupling constant $A_{c,i}$ is proportional to the exchange integral [26]:

$$I_{fs,i} = \int \mathrm{d}\vec{r}_1 \int \mathrm{d}\vec{r}_2\, \psi^*_{nk}(\vec{r}_1)\phi^*_{5f,i}(\vec{r}_2)\frac{e^2}{|\vec{r}_1-\vec{r}_2|}\psi_{nk}(\vec{r}_2)\phi_{5f,i}(\vec{r}_1). \tag{11}$$

$\vec{\psi}_{nk}(\vec{r})$ is a conduction band wavefunction with n the band index and k the electron momentum, $\phi_{5f,i}(\vec{r})$ is the wavefunction of the ith CEF-split 5f-electron state. Usually in the literature the conduction electrons are approximated by plane waves and the integral reduces essentially to the form factor of the 5f-electron density in the limit where the Coulomb interaction is so strongly screened that it can be replaced by $\delta(\vec{r}_1 - \vec{r}_2)$. In any case the integral will be equal for all $\phi_{5f,i}$, and $A_{c,i}$ becomes a constant independent of the level i. In this case equation (9) reduces to the conventionally assumed $K_c = A_c \cdot \chi_{5f}$. However, if $|\psi_{nk}(\vec{r})|^2$ is not assumed to be constant across the crystal, $I_{fs,i}$ may become dependent on the orientation of the density distribution of each state $\phi_{5f,i}(\vec{r})$. An extreme assumption may be that one can replace $\psi_{nk}(\vec{r})$ by a hydrogen like s wavefunction centred at the μ^+-position, since it is known that the screening charge distribution around the μ^+ resembles that of atomic hydrogen [27].

The above scenario would lead to a temperature-dependent and anisotropic ratio of $K_c(T)/\chi_{5f}(T)$. Such behaviour has indeed recently been found in Th-doped UBe_{13} [28], HoB_2C_2 [29] and $PrCu_2$ [30] and possibly other compounds.

A quantitative analysis of the line broadening in the present case is made difficult by the possibility that the presence of the μ^+ modifies the CEF splitting [23] and may also have an effect on the molecular-field parameter λ. Also, our knowledge of the CEF splitting is still incomplete [17]. Moreover, the presence of two distinct U sublattices complicates matters even further. Nevertheless, the scenario that we have described offers a plausible explanation for the appearance of a broadened field distribution at the μ^+-sites.

The measured Knight shifts reflect an average over the distribution in the conduction electron spin polarization at the μ^+-sites and may be less drastically affected by the onset of the quadrupolar order. Nevertheless, anomalies, particularly in K_1 for $H_{ext} \parallel c$-axis, at T_2, T_1 and T_0, are clearly indicating the various phase transitions. Again we are inclined to associate them with the behaviour of the contact hyperfine field.

An interesting question, to be studied theoretically, is whether the observed modulated spin density at the μ^+-sites is only seen because of the modified charge distribution around the μ^+ or whether it is an intrinsic phenomenon connected to the true density distribution of the

conduction electrons. In the latter case, NMR measurements using the ^{105}Pd nucleus should also be able to detect this phenomenon, via a line broadening.

6. Discussion of zero-field and transverse-field results below T_2

The phase transition at T_2 is ascribed to changes in the AFQ structure and the formation of an antiferromagnetically (AF) ordered state involving moments on the quasi-cubic sites of the order of 0.01 μ_B which have a component of their moment oriented parallel to the c-axis [14]. Assuming various simple AF structures we calculate dipole fields of ∼26 G at the e site and 2–8 G at the f_1 site. A random field of 2 G should have lead to a relaxation rate σ of 0.17 μs^{-1}. It is not expected that inclusion of contact fields will change significantly the order of magnitude of the predicted fields. But the ZF data reveal neither a spontaneous precession signal nor any enhanced relaxation rate below T_2 (see figure 7). As mentioned before, the measured relaxation rate of $\sigma = 0.06$ μs^{-1}, corresponding to a field spread of ∼0.7 G, is fully accounted for by the ^{105}Pd nuclear dipole fields. Why do we not see any evidence for a magnetically ordered state? The first possibility is that the ordered moment is much smaller than the suggested value of 0.01 μ_B. In fact the moment would have to be significantly smaller than the nuclear moment of ^{105}Pd, which appears highly unlikely in view of the neutron results [14, 15]. The second possibility is that the ordered moments are not strictly static but fluctuate in a correlated fashion with MHz frequencies. Indeed, the neutron diffraction peaks below T_2 are not resolution limited, indicating that the moments neither are completely static nor exhibit long-range order. This is reminiscent of the situation in UPt_3 where neither in NMR [31] nor in μSR [32] measurements was evidence for the small-moment magnetic order detected, whilst order clearly showed up in neutron and x-ray scattering experiments [33, 34]. This seemingly contradictory situation was explained in terms of the different time windows accessible by the various techniques [35].

The behaviour of K_1 and σ_1 below T_2 also does not necessarily point to the development of a magnetic phase, although on the basis of the neutron diffraction studies in a magnetic field [15] one might expect the appearance of a field-induced, perhaps more truly static, AFM order. As a consequence, a splitting of signals 1 and 2 or at least some additional line broadening may develop below T_2, as already considered in section 5. For $\vec{H}_{ext} \parallel c$-axis (see figure 8) we observe rather temperature-independent $K_1^{\parallel}(T)$ and $\sigma_1^{\parallel}(T)$, with little or no change at T_2, indicating that if an ordered magnetic state is involved, it does not change significantly across T_2. In contrast, for $\vec{H}_{ext} \perp c$-axis (see figure 9), $K_1^{\perp}(T)$ drops from T_2 to 2 K by almost a factor of 1.8, corresponding to a local field change of −9.6 G. In the same temperature range, $\sigma_1^{\perp}(T)$ changes by +0.15 μs^{-1}, which corresponds to change of only +1.8 G in field spread. The average field at the relevant μ^+-site has thus changed much more than the local field spread. It seems impossible to derive a field-induced AFM order which explains the behaviour of K_1 and σ_1 for the two field orientations. Rather, it seems again that the drop in $K_1^{\perp}$ must reflect the contact hyperfine field, i.e. reflects the local spin polarization and its dependence on the type of quadrupolar order. Hence the μSR data confirm at least the primarily structural origin of the phase transition at T_2.

7. Summary

The quadrupolar phase transitions in UPd_3 at $T_0 \simeq 7.6$ K, $T_1 \simeq 6.8$ K and $T_2 \simeq 4.5$ K are found to be strongly reflected in the muon Knight shift and transverse-field relaxation rate (corresponding to inhomogeneous line broadening in the language of NMR), particularly in

the stronger of the two components found in the spin-precession signal. This component arises from μ^+ located at either the f_1 or the e site. We discuss in particular the strongly enhanced line broadening below 10 K and exclude the possibility that it originates from the modulated lattice distortion in the AFQ phase or from a field-induced AFM order below T_0. We also rule out the possibility that it reflects the magnetic susceptibility via the induced dipole fields at the μ^+. We arrive at the conclusion that the line broadening is associated with a non-uniform conduction electron spin density which leads to a spread in the contact hyperfine fields at the μ^+. We conjecture that this non-uniformity originates from the exchange coupling of the conduction electrons, screening the μ^+-charge, with the non-spherical, site-dependent $5f^2$-electron density distribution around the quasi-cubic U sites. The exchange integral depends on the overlap of the non-spherical $5f^2$-electron density distribution (characterized by the quadrupole moment) and the conduction electron density distribution. For a non-uniform conduction electron density distribution this overlap will depend on the relative orientation of the two density distributions. Hence for differently oriented quadrupoles a different coupling to the conduction electrons is envisioned. Consequently in the AFQ phase the contact field at the μ^+ will depend on the orientation of the quadrupole moments on the nearest cubic U neighbours and hence a certain distribution of contact fields will emerge. It would be interesting to see whether a NMR study of the linewidth of the ^{105}Pd nuclear resonance would also show a broadening below T_0.

In addition we report on ZF measurements in the range 2–20 K. We do not find any signature for the presence of a small moment AFM state below T_2. This situation is consistent with the finite correlation length and time observed in the neutron diffraction studies, and appears similar to the case of UPt_3 where it is argued that slow correlated fluctuations lead to a line narrowing in the time window of μSR and NMR, while in the much shorter time window accessible by means of neutrons the order appears essentially static. A definite understanding of our zero result, however, has to await a better understanding of the magnetic state below T_2, still ill characterized.

References

[1] For a general introduction see
Morin P and Schmitt D 1990 *Handbook of Magnetic Materials (Ferromagnetic Materials)* vol 5, ed E P Wohlfarth and K H J Buschow (Amsterdam: Elsevier) p 1
[2] Feyerherm R, Amato A, Gygax F N, Schenck A, Ōnuki Y and Sato N 1994 *Physica* B **194–6** 357
[3] Feyerherm R, Amato A, Gygax F N, Schenck A, Ōnuki Y and Sato N 1995 *J. Magn. Magn. Mater.* **140–4** 1175
[4] Takigawa M, Yasuoka H, Tanaka T and Ishizawa Y 1983 *J. Phys. Soc. Japan* **52** 728
[5] Schenck A, Andreica D, Gygax F N, Pinkpank M, McEwen K A and Amato A 2000 *Physica* B **289–90** 311
[6] Buyers W J L and Holden T M 1985 *Handbook on the Physics and Chemistry of the Actinides* vol 2, ed A J Freeman and G H Lander (Amsterdam: Elsevier) p 289
[7] McEwen K A, Steigenberger U and Martinez J L 1993 *Physica* B **186–8** 670
[8] Andres K, Davidov D, Dernier P, Hsu F, Reed W A and Nieuwenhuys G J 1978 *Solid State Commun.* **28** 405
[9] Ott H R, Andres K and Schmidt P H 1980 *Physica* B **102** 148
[10] McEwen K A, Ellerby M and de Podesta M 1995 *J. Magn. Magn. Mater.* **140–4** 1411
[11] Zochowski S W and McEwen K A 1994 *Physica* B **199–200** 416
[12] Zochowski S W, de Podesta M, Lester C and McEwen K A 1995 *Physica* B **206–7** 489
[13] Lingg N, Maurer D, Müller V and McEwen K A 1999 *Phys. Rev.* B **60** R8430
[14] Steigenberger U, McEwen K A, Martinez J L and Fort D 1992 *J. Magn. Magn. Mater.* **108** 163
[15] McEwen K A, Steigenberger U, Clausen K N, Kulda J, Park J G and Walker M B 1998 *J. Magn. Magn. Mater.* **177–81** 37
[16] McMorrow D F, McEwen K A, Steigenberger U, Rønnow H M and Yakhou F 2001 *Phys. Rev. Lett.* **87** 057201-1
[17] McEwen K A *et al* 2002 in preparation
[18] Abela R *et al* 1999 *Hyperfine Interact.* **120–1** 575
[19] Akishin P G and Gaganov I A 1992 *J. Magn. Magn. Mater.* **110** 175

[20] See e.g.
Schenck A 1999 *Muon Science (Scottish Universities Summer Schools in Physics 51)* ed S L Lee, R Cywinski and S H Kilcoyne (Bristol: Institute of Physics Publishing)
[21] Hahn T (ed) 1987 *International Tables for Crystallography* vol A (Dordrecht: Reidel)
[22] Jacob I, Beeri O and Elish E 1995 *J. Alloys Compounds* **221** 129
[23] Schenck A, Sato N K, Solt G, Andreica D, Gygax F N, Pinkpank M and Amato A 2000 *Eur. Phys. J.* B **13** 245
[24] This picture is analogous to the anisotropic hybridization in CeB_6 between the 4f electron at the Ce site and the 2s and 2p electrons at the boron site recently proposed by
Tsuji *et al* 2001 *J. Phys. Soc. Japan* **70** 41
to explain the angular dependence of the boron NMR frequency shift in the ferroquadrupolar phase of CeB_6.
[25] See e.g.
McLaughlin D E, Peña O and Lysak M 1981 *Phys. Rev.* B **23** 1039
[26] See e.g.
Fazekas P 1999 *Lecture Notes on Electron Correlation and Magnetism* (Singapore: World Scientific)
[27] Schenck A 1982 *Helv. Phys. Acta* **54** 471
[28] Sonnier J E, Heffner R H, McLaughlin D E, Nieuwenhuys G J, Bernal O, Movshovich R, Pagliuso P G, Cooley J, Smith J L and Thompson J D 2000 *Phys. Rev. Lett.* **85** 2821
[29] de Lorenzi F 2001 *Diploma Thesis* ETH Zürich
[30] Schenck A *et al* 2002 in preparation
[31] Kohori Y, Kyogaku M, Kohara T, Asayama K, Amitsuka H and Miyako Y 1990 *J. Magn. Magn. Mater.* **90–1** 510
[32] Dalmas de Réotier P, Huxley A, Yaouanc A, Floquet J, Bonville P, Imbert P, Pari P, Gubbens P C M and Mulders A M 1995 *Phys. Lett.* A **205** 239
[33] Aeppli G, Bucher E, Broholm C, Kjems J K, Baumann J and Hufnagel J 1988 *Phys. Rev. Lett.* **60** 615
[34] Isaacs E P, Zschack P, Broholm C L, Buuns C, Aeppli G, Ramirez A P, Palstra T T M, Erwin R W, Stücheli N and Bucher E 1995 *Phys. Rev. Lett.* **75** 1178
[35] Lee M, Moores G F, Song Y Q, Halperin W P, Kim W W and Stewart G R 1993 *Phys. Rev.* B **48** 7392